Structural and Aerodynamics Analysis on Different Architectures for the Elettra Twin Flyer Prototype

J Intell Robot Syst
DOI 10.1007/s10846-013-9823-9

Structural and Aerodynamics Analysis on Different Architectures for the Elettra Twin Flyer Prototype

M. Battipede · P. Gili · M. Vazzola

Received: 11 February 2011 / Accepted: 19 February 2013

Abstract In this paper, the authors analyze and compare two airship configurations for the Elettra Twin Flyer prototype, an innovative airship concept which is remotely-controlled and intended for monitoring, surveillance, exploration and reconnaissance missions. The aim of the comparison is to determine the most appropriate solution in terms of performance, cost and maneuvering capabilities. In particular two potential solutions are analyzed: the first consists of a double-hull configuration, characterized by the presence of a primary support structure connected to a couple of twin inflatable hulls. The second architecture is a soap-shaped exoskeleton configuration which features a single inflated section, incorporating two separate elements, which are held internally by a system of ribs.

M. Battipede · P. Gili · M. Vazzola (✉)
Aeronautical and Space Department, Politecnico di Torino, 10129 Torino, Italy
e-mail: matteo.vazzola@polito.it

M. Battipede
e-mail: manuela.battipede@polito.it

P. Gili
e-mail: piero.gili@polito.it

Published online: 13 March 2013

Keywords UAV · Airship · Structural analysis · FEM · Aerodynamic analysis · CFD

1 Introduction

The low-cost multi-purpose multi-mission platform Elettra-Twin-Flyer (ETF) is being developed through the synergy of Nautilus S.p.A and the Politecnico di Torino [1]. This is a very innovative remotely controlled airship, which is equipped with high precision sensors and telecommunication devices. Because of its peculiar features, it is particularly suitable for inland, border and maritime surveillance missions and for telecommunication coverage extensions, especially in those areas which are either inaccessible or without conventional airport facilities and where the environmental impact is an essential concern [2–4].

ETF is characterized by great maneuverability and low wind sensitivity [5]. The flight conditions range from forward, backward and sideward flight to hovering, both in normal and severe wind conditions. In order to achieve these capabilities the ETF has been conceived with a highly non conventional architecture. The key point of the design is the innovative command system, which is based completely on thrust-vectoring propellers that are moved by means of electrical motors, which are powered by hydrogen fuel cells.

Flight tests are currently in progress on a flight demonstrator [6], which is a reduced-scale reduced-complexity platform, purposely assembled to test the most critical subsystems, such as the command system and the architectural solution. The demonstrator architecture is shown in Fig. 1.

With appropriate axis rotation and variation of the rotational speed of the six propellers, this configuration enables control in 6 Degrees-of-Freedom (DOF). The command system does not need to have a relative speed to be effective, which is a necessary condition to guarantee real hovering capabilities. Moreover, this command system has been conceived to be oriented in the wind direction, so that this airship can point its payload towards a given target regardless of the wind direction, both in hovering and forward flight.

The control procedure, for the demonstrator, is carried out by the pilot action on the cockpit ground station, which consists mainly of two throttles and a three-DOF joystick. The pilot's inputs are first transmitted via a radio-link to the airship platform and then processed and re-allocated by the Control Allocation System [7], which is integrated in the on-board computer [8] of the ETF demonstrator. Successively, these processed signals can be fed to the control boards of the propulsion and orientation motors, in terms of propeller rotational speeds and orientations of the vertical arms. In particular, the joystick can be used to command the orientation of the four thrust-vectoring propellers for lateral and directional manoeuvres, as well as the differential variation of the angular rate of all the six propellers for longitudinal manoeuvres. Conversely, the two throttles act on the collective rotational speed of the four thrust-vectoring propellers and the two vertical axis propellers. In terms of propulsive action, vertical control is obtained through the coordinated and collective action (same thrust level) of the propellers located in the structure that connect the two hulls (vertical axis propellers). The longitudinal control is basically achieved through a differential variation of the rotational speed of the upper and lower propellers; the front and rear vertical axis propellers might contribute in case of necessity and in particular when the airship is engaged in high speed regimes, when the horizontal axis propellers (upper and lower) are all saturated to obtain the necessary forward thrust. At low or zero speed this might imply that a set of propellers needs to work at reverse speed, to obtain a negative thrust and, thus, a pitching moment. The lateral-directional control is obtained through a differential rotation of the forward propellers: with uncoupled commands the propeller arrangement involves, for the lateral command, the upper propellers thrusting in one direction and the lower propellers in the opposite direction; whereas the directional command is obtained by making the front propellers (upper and lower) thrust in one direction and the back propellers (again upper and lower) in the opposite direction. Usually, however, the commands are coupled, and the real arrangement is a combination of the above mentioned schemes [9].

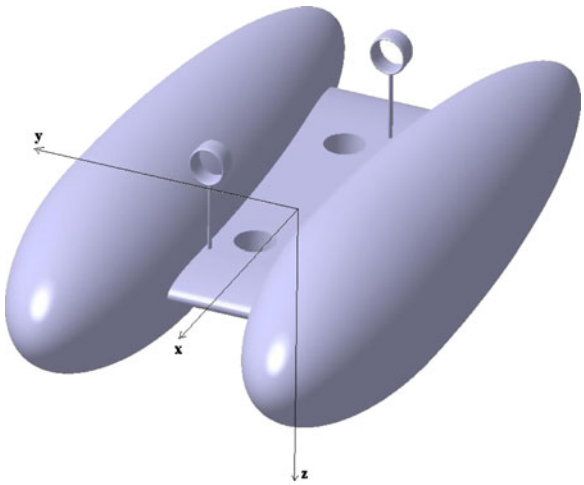

Fig. 1 Elettra Twin Flyer demonstrator

During hovering, altitude is maintained through the synergy of the helium buoyancy and the thrust of the vertical propellers. Forward movement creates an additional aerodynamic lift which is generated as a result of the air-flow circulation over the hulls. The complete absence of aerodynamic control surfaces not only increases manoeuvrability at low speed, but also eliminates a source of disturbance during operation in adverse weather conditions. An obvious consequence of this approach is that a higher power consumption is required to manoeuvre and, as power is limited and must be shared between propulsion and manoeuvre,

a reduction in manoeuvrability is clearly experienced at high speed. However, these drawbacks have been considered perfectly acceptable, for the range of applications for which this airship has been conceived.

2 New Airship Configurations

Ground and flight tests are revealing that the architecture can be further optimized. The demonstrator, in fact, had been conceived to demonstrate the effectiveness of the control architecture and with specifications typical of a test bed: it did not have to accommodate any payload, whereas system accessibility was fundamental, in order to facilitate the installation and the setting of new components being tested. The avionic architecture versatility was also a requirement, even though it implied scarce reliability, associated to the extra burden of cables and connectors which could be otherwise avoided. To respond to operative requirements typical of a series product, the whole configuration is now being reconsidered. Different architectures have been proposed and they are now being analyzed from manifold points of view, considering the same mission and design requirements. These are the very same requirements as those stated for the original ETF configuration [5], which were initially identified as a result of a market survey. The criteria used during the evaluation phase will be highlighted in the next section.

Generally speaking, the new configurations are evolutions of previous designs whereas the control system strategy is the same, in spite of the different number of propellers. These can be 8 or 10, 2 or 4 of which are fixed whereas 4 or 8 are manoeuvrable. As for the previous configuration, the new ETF06 does not have movable aerodynamic control surfaces.

Low environmental impact is guaranteed through the employment of electric motors as well as the power system, which is based on hydrogen fuel cells and auxiliary batteries or supercapacitors which supply extra energy to compensate for the peaks that occurs because of abrupt manoeuvres.

Fig. 2 Non-rigid double-hull configuration

In order to make the aerodynamic and structural analyses cost-effective, two configurations have been selected as the most representative. The two alternative solutions can be described as following:

- The first one is a direct derivation of the demonstrator—the *double-hull* solution (Fig. 2). This is characterised by a main structure, connected to the two gas envelopes by means of a set of elongated S-shape clamps. These clamps are rigid and dimensioned to sustain the propeller longitudinal loads and transfer the aerodynamic loads to the main structure. Of all the available aeronautical technologies, aluminium truss and carbon sandwich structures have been considered.
- The second solution is distinctly different from the demonstrator, above all because it is a rigid structure—this is known as the *soap-shaped* or *exoskeleton* design (Fig. 3). It features a single hull formed through the union

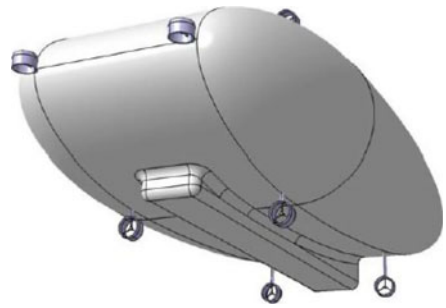

Fig. 3 Rigid soap-shaped configuration

of two parallel hulls, supported internally by a system of structural ribs. The *double-hull* structure is too complex to be made with standard aluminium components, therefore only the carbon sandwich solution has been analysed.

3 Cost Function Definition

In order to select the best solution, a cost function has been introduced to take into account a number of design criteria [10], which should identify the best performance-over-cost ratio. Each criterion is weighted according to its relative importance in the overall design. Five different weight indexes are considered: low, medium-low, medium, medium-high and high, all scaled with respect to the maximum 'high' level, which assumes a unitary value. At the end of the process each configuration should be associated with an objective index which indicates the design excellence.

The following factors have been considered:

- overall dimension: the assumption is that the cost function varies linearly with the overall dimension; the associate cost weight is selected to give the parameter medium-high importance;
- weight: evaluated as the overall dimension, but with medium-low importance;
- wind sensitivity: as this is an aerodynamic consideration it is evaluated in terms of aerodynamic stability derivatives. The cost function has a quadratic relationship with the wind sensitivity which is weighted to give the parameter high importance;
- handling and payload accommodation: since, in both cases, it is difficult to define a parameter that represents these criteria effectively, they are weighted as a linear cost and a medium importance is assigned;
- acquisition and operating costs: the parameter is weighted linearly with a medium-high importance;
- reliability, service life and maintenance (cost, mean time to repair, mean time to service…): these are parameters that can be considered similar if not equal for both solutions. As improvements of these parameters clearly imply increases in the design and production costs, they have been considered as linearly-increasing costs and medium-high importance has been attributed to each of them.

4 Double Hull Configuration

The double-hull configuration (Fig. 2) is the classic design of two hulls separated by a central structure: the *nacelle* (the compartment in which the payload, power supply and avionics are located) is positioned beneath the line of contact between the two hulls, enabling television cameras, if installed, to be tilted and pointed downwards without any visual obstruction. Two large vertical propellers are positioned at the fore and aft ends of the central structure. Eight longitudinal–axis propellers are used for propulsion and orientation. They could be reduced to four which is the minimum number of effectors required for full maneuverability. The connecting structure is a central tube that runs in the longitudinal direction between the two S-shaped arms, which are rigid and are used to support the propellers (Fig. 4).

This shaft is partitioned into five sections, corresponding to the couple of S-shape forceps and the three intermediate ribs which support the nacelle.

The hulls are secured to the structure through straps, which are fastened at all of the five connection points. In this way the most critical loads, which are caused by the buoyancy, can be uniformly distributed along the main resistant direction of the belt, whereas the aerodynamic forces are transmitted to the S-shaped structures. The same structures prevent the hulls from being pushed and eventually unhinged from their location. The aerodynamic drag, in fact, is contrasted by the belt friction and, even more important, by the clasp action exercised by the counteracting Ss, which embrace the hulls on the two sides of the maximum diameter section.

The central shaft is the part onto which all the other components are attached. Its length is proportional to the sum of the two semi-axes of the ellipses that constitute the hulls (around 0.6

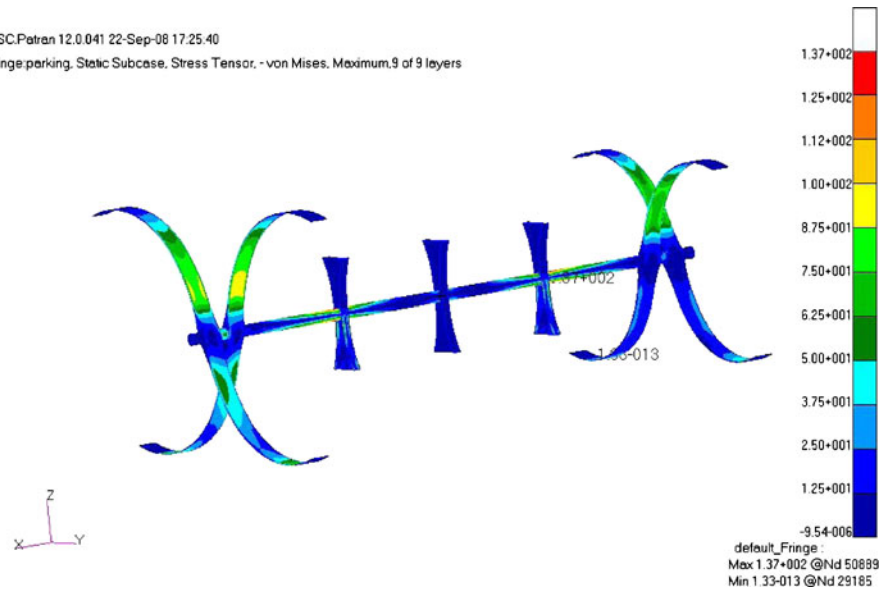

Fig. 4 Structure of the non-rigid double-hull configuration (stress tensor values range from 0 to 137 N/mm^2)

times the total length). It must be sufficiently long to space the supporting arms.

The supporting arms represent the most critical part of the design and, due to their long and slender shape, are likely to experience the most severe deflections. Excessive deformations should be carefully avoided to maintain the thrust forces in the nominal positions and minimize control discomfort. The central septa have two main functions: the first concerns the hulls, as, together with the supporting arms, they help maintaining the envelopes rigidly connected to the structure. The second function is to support the nacelle underneath.

In the model created for the structural simulation [11, 12], the nacelle was assumed to hang from the septa in the space between the two hulls and the connection was simulated with rigid elements. As with the supporting arms, the septa were intentionally designed to have three planes of symmetry.

The shape of the hulls have been determined on the basis of aerodynamic considerations. It is, in fact, very well known that, for a single hull, the aerodynamic drag is influenced to a great extent by the slenderness ratio (length over radius). The slenderness ratio was therefore selected to minimize the drag over the whole speed envelope [13]. For the same reason it was decided to make the hull longitudinally non symmetrical [13, 14], shaping the longitudinal section as two half-ellipses, one with its major axis equal to a third of the total length of the airship and the other with the major axis equal to the remaining two-thirds of the length. The minor axes are clearly coincident and equal to approximately one-eighth of the total length. The overall hull was then designed as a revolution of the longitudinal section, whose dimensions had to be calculated iteratively, as they affect two design parameters: the volume of helium that can be contained (and hence the aerostatic lift) and the surface area of the hulls, which is necessary to calculate the total mass.

5 Soap-Shaped (Exoskeleton) Configuration

The second configuration is the exoskeleton (Fig. 3), which is formed by merging the two hulls in a central inflatable body. The main advantage of this configuration is that, for an equivalent length, the helium volume increases by about 20 %, and this corresponds to a beneficial buoyancy increase. At least in theory, this leads to two possibilities: an increase in the payload capability or a decrease in the overall dimensions. What actually happens, however, is that the exoskeleton

structure has a mass which is much greater than the double-hull one of the same length.

The structure of the exoskeleton is geodesic, and is made up by eight "ribs" constituted by T-section curved beams (Fig. 5). The T-section has been selected as the lightest feasible solution, to support local loads in 6 degrees-of-freedom. There are four vertical propellers, positioned at the prow and the stern and along the sides of the airship, in addition to the 8 (or at leas4 t) thrust vectoring propellers, which are positioned in the same way of the double-hull configuration. The exoskeleton offers more degrees of freedom for propeller positioning, as any longitudinal spar could virtually be used as a support. Despite this, the number of propellers is reduced from eight to four—two of which are positioned on the dorsal part of the airship and the other two on the ventral part, all aligned in the xz plane of symmetry. The nacelle is still positioned underneath the hull, in the same way of the double-hull configuration.

The envelope is no longer a single multi-layer fabric: the functions of the multi-layer, in fact, can be performed through the action of two separate envelopes, an internal bladder and an external structural fabric, which has the main task of resisting the atmospheric agents, while dispersing water and static electricity. This solution is more cost effective and leads to a reduction in the fabric weight per square feet, compared to the multi-layer solution which has to be employed for the *double-hull*.

As far as the overall weight of the structure is concerned *soap-shape* offer a slight advantage over the *double-hull* shape. The structure weight represents one of the parameters that is weighted in the cost function (Table 4), and is associated to the buoyancy necessary to hover at sea level, which represents the total weight. The ratio of the operating empty weight over buoyancy shows the same trend with a slightly favorable value of 0.75 for the *soap-shape* against the value 0.8 for the *double-hull.*

There are two main causes of deformation in the exoskeleton design: the buoyancy that acts upwards on the upper surface of the airship envelope, and the weight of the nacelle that acts downwards on the bottom part of the structure. The result is a dilation of the structure along the vertical direction, which results in deformations greater than 1 m. In order to reduce this effect, the upper and lower parts of the ribs and spares are constrained by a set of restraining cables in the vertical-longitudinal plane. The cables are incredibly effective and introduce a negligible mass increase (about 10 kg). The only drawback is that, from the practical point of view, each cable must be sealed to the inner bladder, which should still be able to maintain its helium retention capabilities.

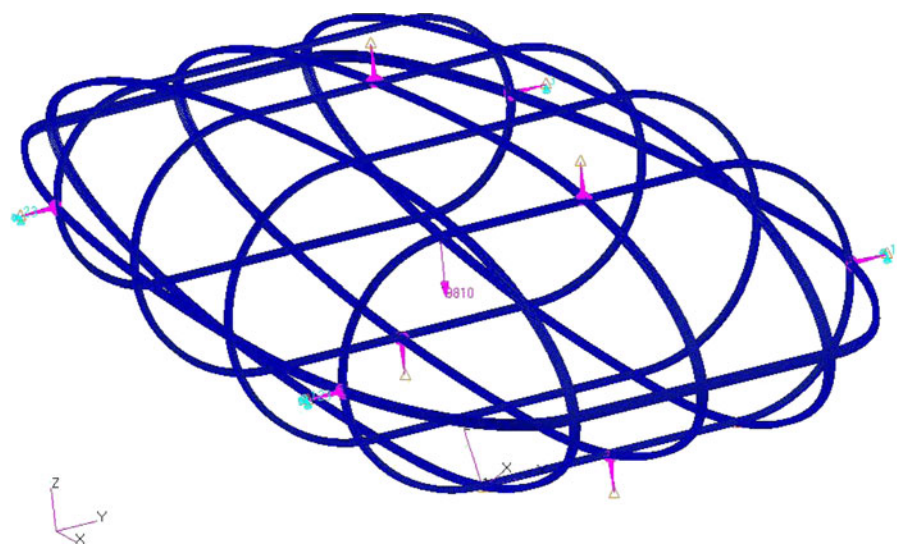

Fig. 5 Exoskeleton of the soap-shaped configuration

6 Fluid Dynamic Analysis

A preliminary fluid dynamic analysis [15] has been performed on the two different architectures using a commercial code (STAR-CCM+) [16] that solves the complete set of Navier–Stokes equations on structured/unstructured computational domains, using a finite volume method. This program is able to perform the unsteady analysis as well as to evaluate the interaction between the aerodynamic field and structural vibrations.

The Steady Reynolds-Averaged Navier–Stokes (RANS) equations have been solved using the sequential algorithm based on the Semi-Implicit Method for Pressure Linked Equations (SIMPLE) [17] method with a second order discretization model on a polyhedral mesh.

A realizable k-ε turbulent model has been used with a suitable wall functions model.

The geometrical dimensions of the domain, compared to the length of the airship, are large enough to prevent the flow field around the airship from being affected by numerical external conditions (Fig. 6).

The software provides, of course, the generation of a grid mesh which is, for both models, a full polyhedral mesh having the following features:

- *double-hull* (Fig. 7): numbers of cells $\sim$ 3.5E6
- *soap-shaped* (Fig. 8): numbers of cells $\sim$ 3.0E6

The main purpose of the fluid dynamic analysis is to evaluate the aerodynamic coefficients for different Reynolds numbers. These coefficients are meant to be included, in look-up table form, in the aerodynamic data-base of the ETF Flight Simulator [18], which provides an effective and strategic tool for the design and testing of the innovative flight control system.

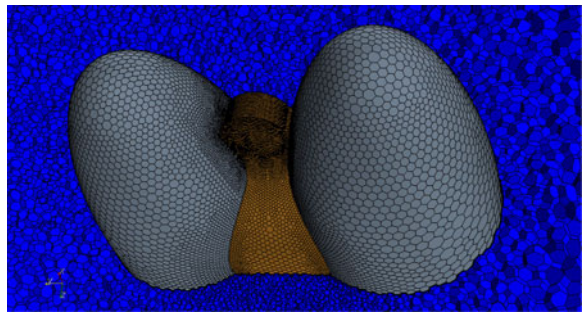

Fig. 7 Double-hull mesh

The look-up tables currently used on the ETF Demonstrator Flight Simulator are very large. Several different flight speeds are considered for each of the 6 aerodynamic coefficients (C_x, C_y, C_z, C_{Mx}, C_{My} and C_{Mz}), in order to evaluate the influence of the Reynolds number. Considering the two planes of symmetry (x-y and x-z) and the ability of the airship to move in any direction, it was decided to perform the aerodynamic analysis over the following ranges: $0° \leq \beta \leq 180°$ and $0° \leq \alpha \leq 90°$. With this requirements, it is clear that, in order to span the whole flight envelope, a complete aerodynamic analysis requires at least 120 test points for each speed: very low speed ($V = 2$ m/s), speed near to the maximum vertical climbing rate ($V = 4$ m/s), speed near to the maximum wind speed in hovering, maximum rate of descent ($V = 8$ m/s) and speed near to the maximum flight speed ($V = 20$ m/s). For a preliminary analysis, however, it was decided to reduce the number of points to 21 and to just one

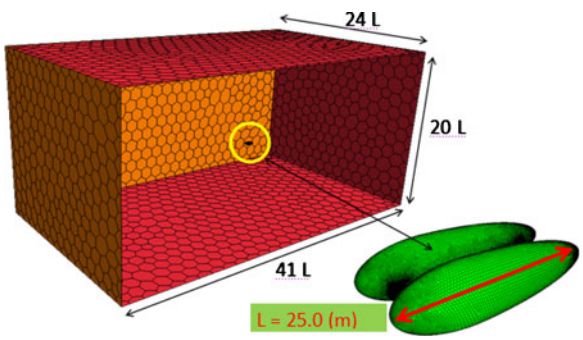

Fig. 6 Computational domain

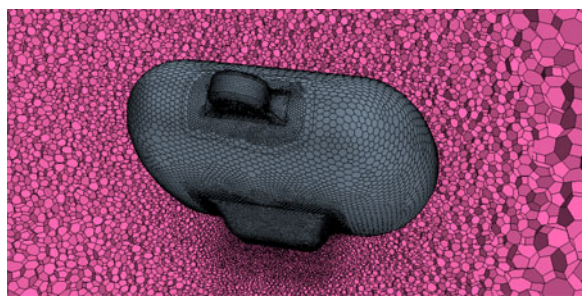

Fig. 8 Soap-shaped mesh

(low-medium) speed value ($V = 10$ m/s), even though further information for lower Reynolds numbers is highly recommendable, as a large part of an airship mission is performed at very low speed, in a laminar flow.

In order to reduce the computational cost, a Coarse Mesh has been used (Cell Number $\sim$ 3E6). Considering the preliminary state of the design, this was considered a fairly good compromise between computational costs and numerical accuracy.

In both cases, the nacelle takes up a volume of 1/40 of the gas volume. A length of 25 m was considered for both the solutions. The effective dimensions, however, have actually little importance for the comparison, as the results are given in non-dimensional form.

A body reference frame has been adopted for the aerodynamic analysis: this is based on three orthogonal axes with the origin (O) in the longitudinal plane of symmetry, located centrally along the maximum overall length of the airship. In other words:

- the X axis lies in the longitudinal plane and is oriented towards the airship prow;
- the Z axis is oriented downwards and contained in the longitudinal plane of symmetry;
- the Y axis is positive starboard, and form a right-handed reference frame.

The components of the speed vector V are calculated according to the scheme of Fig. 9:

$$u = V \cdot \cos\alpha \cdot \cos\beta$$
$$v = V \cdot \sin\beta$$
$$w = V \cdot \sin\alpha \cdot \cos\beta$$

where u, v, and w are, the linear speed components in the x, y and z body-axis reference frame, respectively.

The wind and body axes have the same origin and precisely, the wind axes are rotated with respect to the body axis, in order to present:

- the X axis aligned with the speed vector V direction, but with the opposite sign;
- the Z axis contained in the airship longitudinal plane of symmetry, oriented downwards
- the Y axis as a consequence, to form a right-handed reference frame.

The most interesting results of the comparison between the two solutions are reported in the following section.

- Aerodynamic Performances

The comparison of the aerodynamic coefficients provides information that can be used to evaluate the aerodynamic performance of the two solutions in specific flight conditions. Figure 10 shows the trend of the X-wind force as a function of the angle-of-attack α (for $\beta = 0°$). In particular, for $\alpha = \beta = 0°$, the difference between the two configurations is almost undetectable on an overall scale: a more accurate analysis of the force values, however, reveals that the aerodynamic force along the X-wind axis is 20 % lower for the soap-shape solution (for the same overall length L). For example, with an overall length of 25 m, the drag is, approximately, 139 N for the soap shape and 174 N for the double hull. The pressure coefficient contour plot and the iso-surface $Cp_{tot} = 0$ (separated flow), for this flight condition ($\alpha = \beta = 0°$),

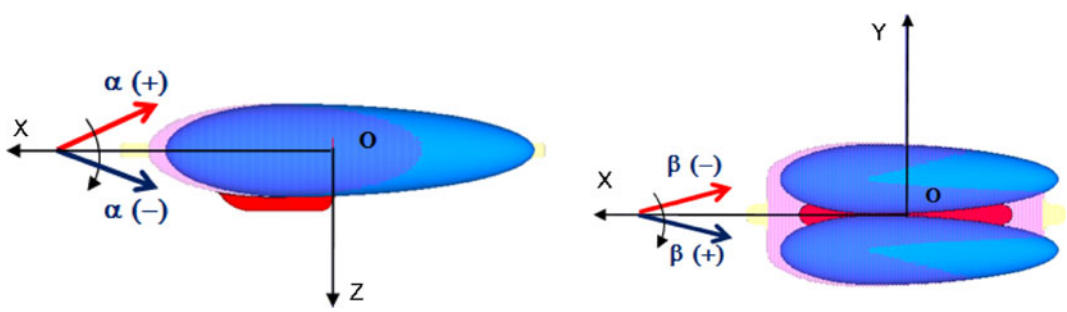

Fig. 9 Reference system and notations

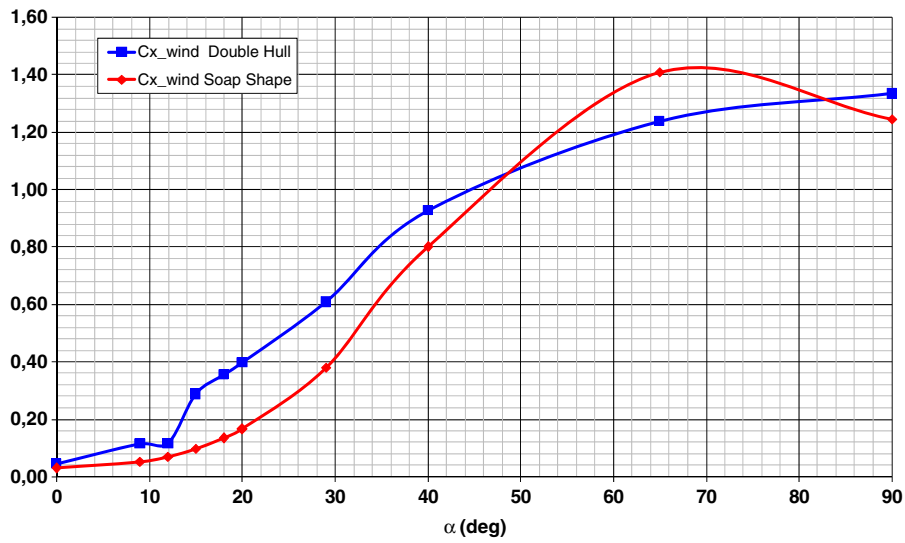

Fig. 10 Cx in wind axes vs. angle α

are reported in Fig. 11, for the two configurations. Cp_{tot} can be defined as:

$$Cp_{tot} = \frac{p_{tot} - p_\infty}{\frac{1}{2} p_\infty V_\infty^2} = Cp + \frac{V^2}{V_\infty^2}$$

where p_{tot} and V are the total pressure and the fluid velocity at the point in which the pressure coefficient is being evaluated, whereas p_∞, ρ_∞ and V_∞ are the freestream (i.e. remote from any disturbance) pressure, fluid density and fluid velocity, respectively. In particular, the $Cp_{tot} = 0$ condition is verified when the flow separates: the static pressure acquires the same value as the undisturbed fluid and the relative speed is suddenly reduced to zero (stagnation point). It can

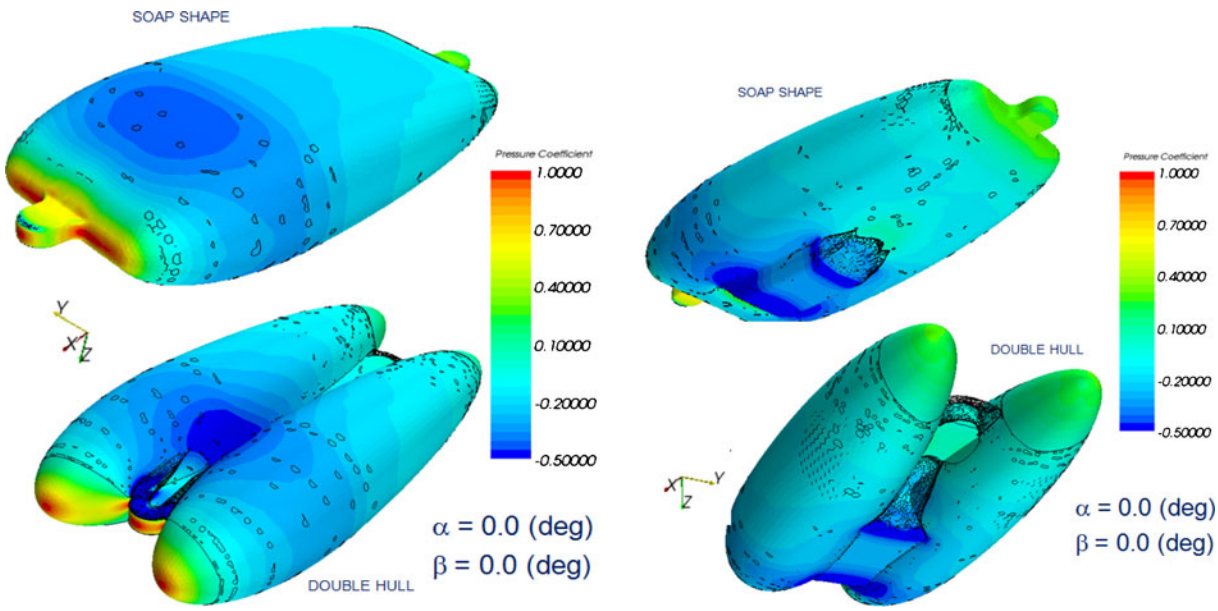

Fig. 11 Contour of pressure coefficient & Iso_surface $Cp_{tot} = 0$

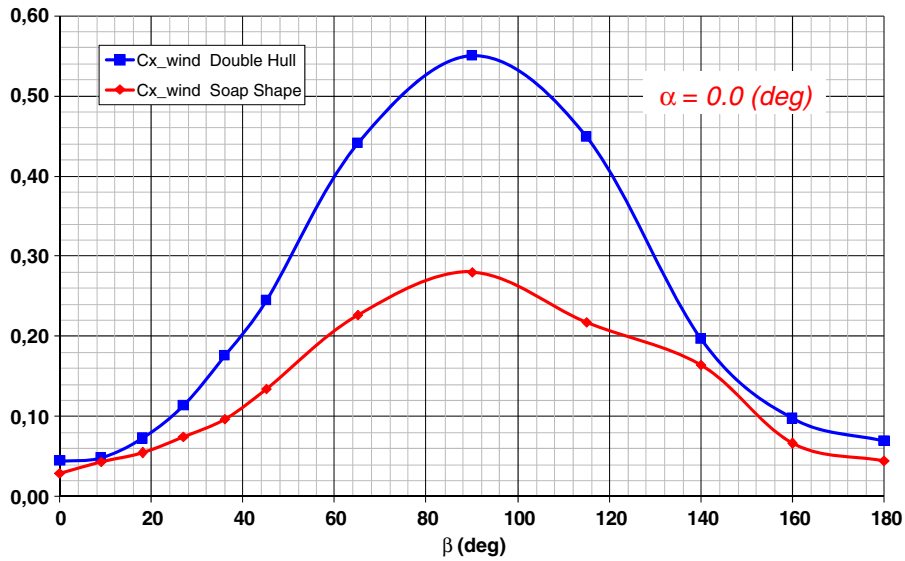

Fig. 12 Cx in wind axes vs angle β

be noted that the pressure distribution and the wake structure for the two architectures are very different, especially in the central zone, but this has little influence on the drag value.

The same plot in Fig. 10 provides information on the drag action on the two bodies in a vertical descent situation ($\alpha = 90$ deg): in this case, the soap-shape solution has a drag value higher by about 12.5 %.

The plot in Fig. 12 shows the force coefficient along the X wind axis as a function of β for $\alpha = 0°$ and provides information on drag for different sideslip angle values. In particular, in a cross-wind situation of ($\beta = 90°$), the value of the drag coefficient (and therefore of the thrust required to hover with a side wind) is very different for the two solutions with a peak that is about 40 % lower than that of the double-hull configuration. The aerodynamic behaviour of this flight condition is shown clearly in Fig. 13, in which the pressure coefficient contour plot and the iso-surface for $Cp_{tot} = 0$ are reported. It can be noted that

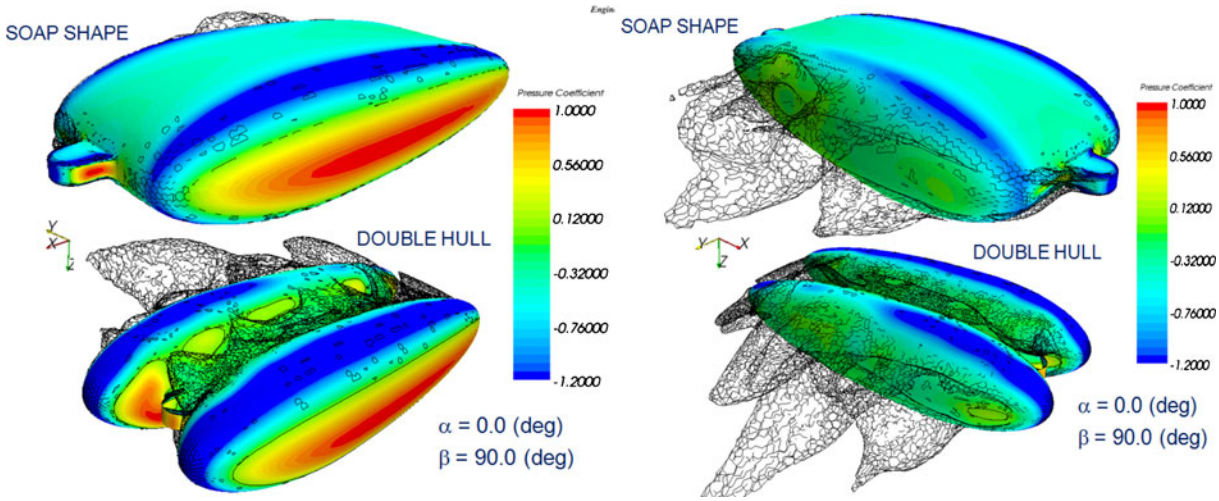

Fig. 13 Contour of pressure coefficient & Iso_surface $Cp_{tot} = 0$

the double-hull configuration shows larger a high pressure zone than the soap-shape and a more extended wake structure. These two circumstances are the main reasons for the increase in drag.

The numerical investigation clearly demonstrates that there is a distinct advantage from an aerodynamic point of view, for the exoskeleton design, in particular in the "cross-wind" situation (Fig. 13). The value of the drag coefficient C_x for the sideslip angle $\beta = 90°$ (Fig. 12) is clearly representative of this phenomenon and, for this reason it was selected to represent the wind sensitivity factor in the cost function.

- Static Stability

Static instability is the natural disposition of a dynamic system to depart from a condition of equilibrium after a small disturbance. The sign of the stability coefficients, and their values, can offer useful information about this disposition. Longitudinal stability can be defined by the derivative:

$$\frac{\partial C_{My}}{\partial \alpha}$$

According to the definition of positive moments and angles, this derivative must be negative to have longitudinal stability. In the same way, the tendency to reduce or increase disturbances on the lateral and directional planes can be defined by the derivatives:

$$\frac{\partial C_{Mx}}{\partial \alpha} \text{ and } \frac{\partial C_{Mz}}{\partial \beta}$$

Accordingly, they must be positive to have lateral and directional stability.

The numerical analysis performed on the two configurations have confirmed a trend which is very well known in literature, the hull, in fact, is statically unstable, in pitch, with a natural inversion of the o stability coefficient sign for very high values of the angle-of-attack (>45) [19]. For this reason, a longitudinal Stability Augmentation System (SAS) is strongly recommended, as already shown for the demonstrator [20].

The longitudinal stability coefficient has been compared for the two solutions over the whole angle-of-attack range, as shown in Fig. 14, as qualitative differences can be detected in the two trends. The double-hull configuration, in fact, presents:

- an irregular trend;
- a lower maximum value;
- a lower slope for very low angle-of-attack values (around $\alpha = 0$).

Such behaviour can be explained through the analysis of Fig. 15, which shows that, for an angle-of-attack of 15°, a separation starts in the central

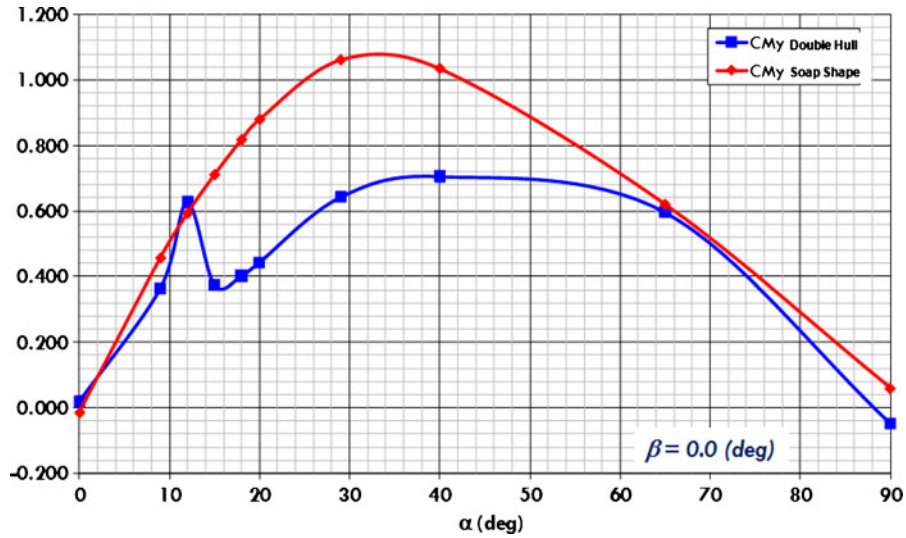

Fig. 14 Pitching moment coefficient; C_{My} vs. α

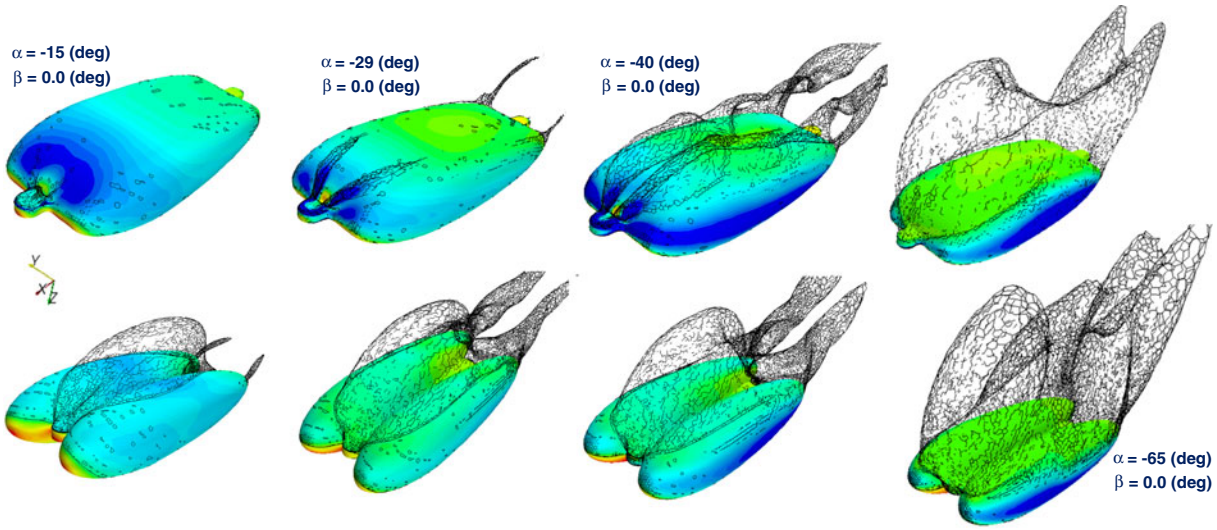

Fig. 15 Wake evolution

part of the double-hull configuration, and this leads to a considerable reduction of the aerodynamic moment. The separation region spreads to the hulls when the angle-of-attack increases, until, at about 65°, it incorporates the wake vortexes. On the soap-shape configuration, separation takes

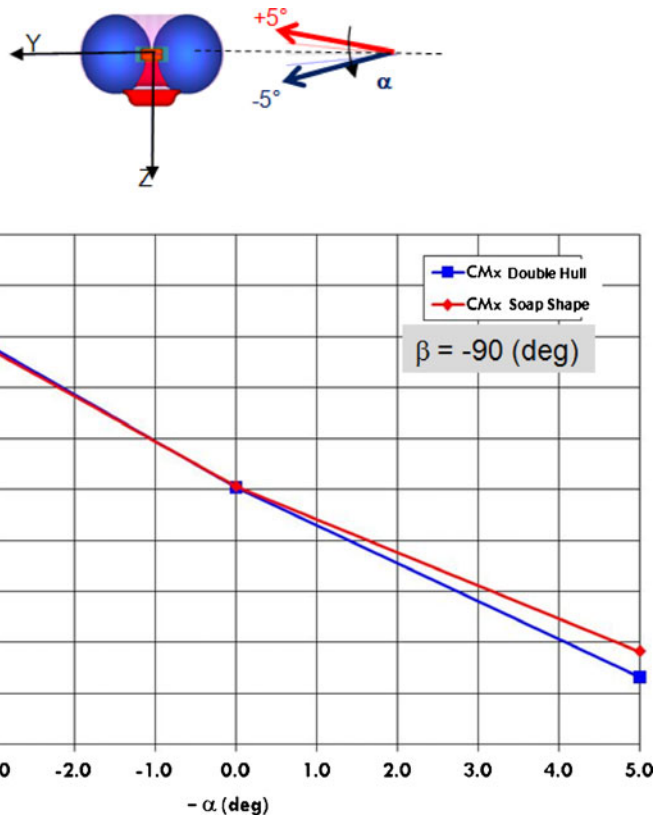

Fig. 16 Rolling-moment coefficient: C_{Mx} vs. α

place between 30 and 40°, with a considerably smoother process.

The results presented in Fig. 14, could be interpreted erroneously as it could seem that the flow separation has a beneficial effect on the static stability, as the curve slope is slightly lower on the double-hull configuration, and it also features a negative trend between about 11 to 15°. It should be noticed, however, that the curve irregularities expand the instability region, delaying the trend inversion to about 65°, whereas the stability region on the soap-shape configuration is reached much earlier (between 30 and 40°). Moreover, as shown in Fig. 10, the flow separation leads to a great deal of extra aerodynamic drag.

As far as lateral-directional stability is concerned, two aerodynamic derivatives are considered: $C_{Mx_\alpha} = {}^{\partial C_{Mx}}/_{\partial\alpha|_{\text{trim}}}$, for the trim condition $\alpha = 0°$ and $\beta = 90°$ and $C_{Mz_\beta} = {}^{\partial C_{Mz}}/_{\partial\beta|_{\text{trim}}}$ for the trim condition $\alpha = 0°$ and $\beta = 0°$. The first one represents a particular hovering condition, that is made possible by the unique ETF trust vectoring command system; the second one is a common forward flight condition, which can be considered qualitatively representative of a wider angle-of-attack range. In order to evaluate the above-mentioned derivatives, the rolling moment and the yawing moment coefficients have been calculated in the proximity of the two trim conditions, according to the small theory approximation method.

Figure 16 shows the rolling moment coefficient in the cross-wind situation ($\beta = 90°$) in the proximity of the trim point $\alpha = 0$ deg: the trend reveals static instability also on the lateral-plane and this is the reason why the lateral dynamic behaviour should also be augmented by means of a dedicated SAS. It is interesting to notice, however, that the instability level is almost the same for the two solutions, as can be observed from the slopes of the two curves.

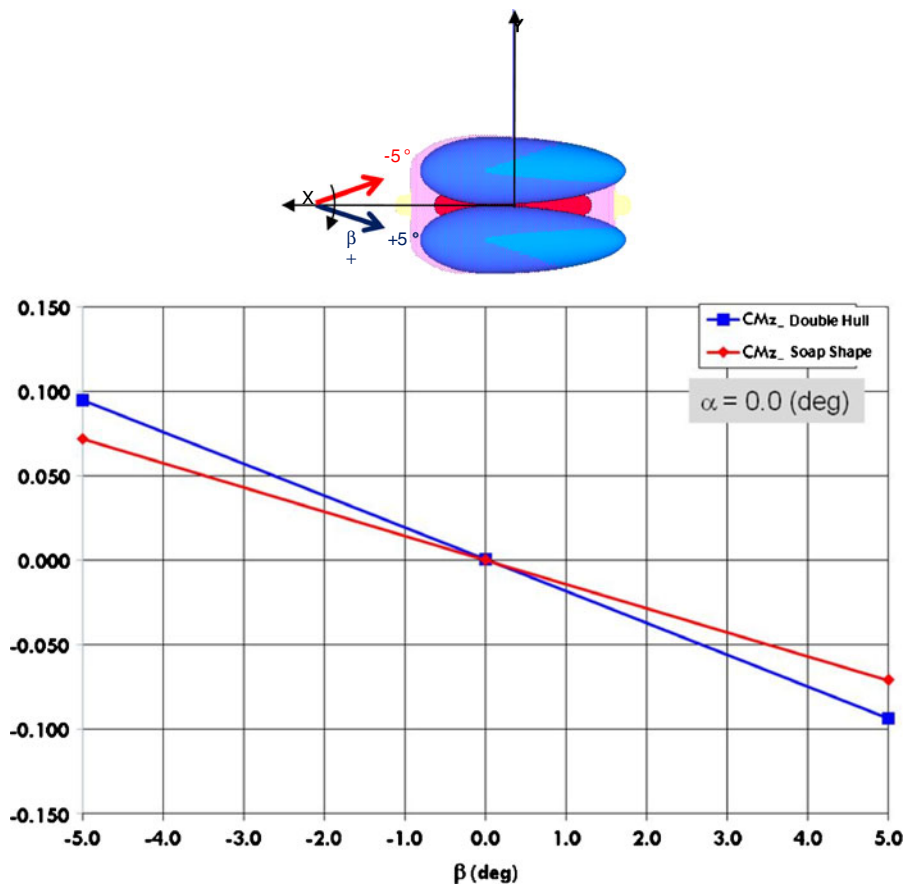

Fig. 17 Yawing-moment coefficient: C_{Mz} vs. β

As far as the directional behaviour is concerned, the situation is highlighted in Fig. 17 in which a slightly favourable condition for the soap-shaped solution can be noticed: again, the absolute value shows instability, but the slope of the related curve is lower for the soap-shaped configuration.

From the airship stability point of view, there are no specific reasons why one configuration should prevail over the other.

- Unsteady Analysis

The unsteady RANS equations have been solved using the sequential algorithm based on the SIMPLE method [16], with a second-order discretization model, implemented with the same commercial CFD solver STAR-CCM + used for the steady analysis. The aerodynamic/numerical analysis has highlighted remarkable oscillations of the force and torque coefficients in the cross-wind situation for the double-hull configuration. The $\beta = 90°$ point originates instability phenomena and the analysis of the steady condition shows convergence problems. For this reason, it has been chosen to perform an unsteady analysis and to calculate the aerodynamic coefficients as the mean values over a limited time window (Fig. 18). The problem is far less evident for the soap-shape configuration. A further analysis of Fig. 16 would be useful to explain the phenomena associated to the presence of the two hulls. Apart from the downstream wake, in fact, there is the additional contribution of the flow separation in-between the two hulls, which accentuates the vortex strength. The increase in drag shown in Fig. 12 is not the only drawback. If the frequency of the aerodynamic oscillation overlaps the structural natural modes, in fact, the phenomenon could degenerate into devastating aero elastic instabilities which could lead to critical structural damage.

The time-histories of Fig. 18 have been obtained for a constant forward speed of 8 m/s: it

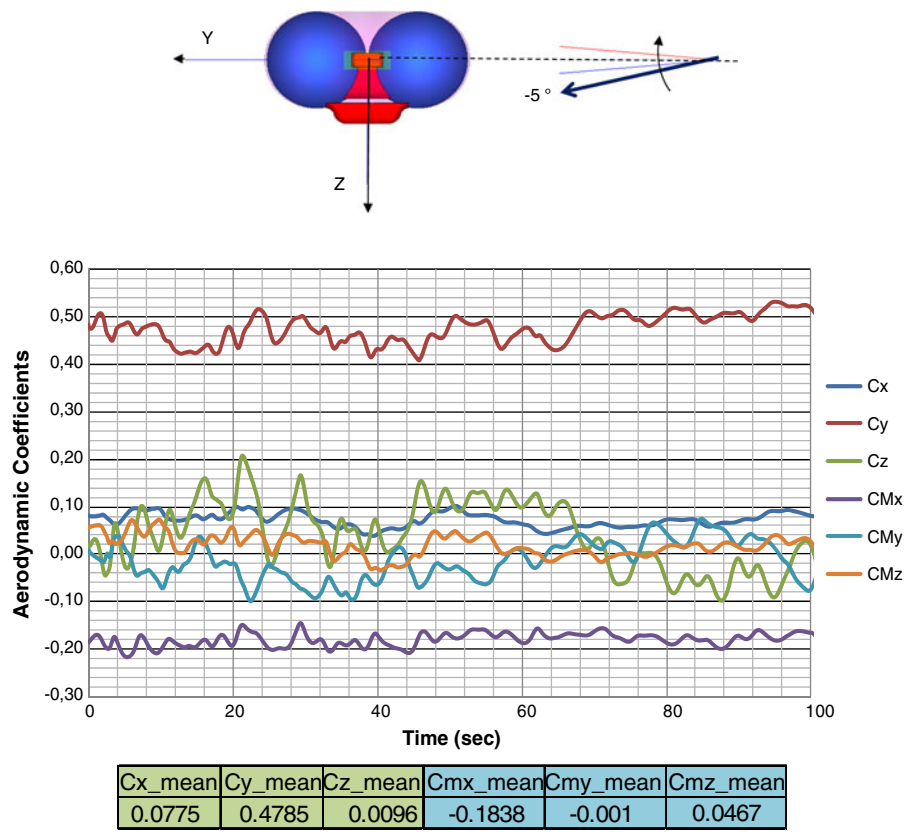

Cx_mean	Cy_mean	Cz_mean	Cmx_mean	Cmy_mean	Cmz_mean
0.0775	0.4785	0.0096	-0.1838	-0.001	0.0467

Fig. 18 Aerodynamic coefficients vs. time unsteady simulation—$\alpha = -5$ (deg); $\beta = 90$ (deg)

is possible to observe a coefficient frequency oscillation of about 0.3 Hz, which corresponds to a Strouhal number of approximately 0.23 (calculated with the characteristic length equal to the maximum airship height $-d = 6.26$ m).

$St = 0.23$ is very close to the characteristic value of $St = 0.18$ at which the vortex unsteady separation phenomenon starts to be detectable on sharp-edge obstacles.

Both the static and dynamic analysis have highlighted that the exoskeleton design is more favourable from an aerodynamic point of view.

7 Structural Analysis

The two different structural solutions which have been considered, have the same tasks: they have to transmit all the airship manoeuvring actions generated by the trust-vectoring propellers, collect the aerostatics forces generated by the helium and provide the onboard systems, payloads and power unit with the appropriate attachment points and housing.

The action of the command system is perpetrated by the forces produced by the propellers, which have to generate high rotational moments. For this reason, they must be positioned far from the centre of gravity. Moreover, both solutions have to be dimensioned with the constraint of maintaining the applied forces at fixed positions, in order to ensure a correct control action. The resulting structures have to be characterized by high rigidity and very low stress levels. A thorough analysis of the propulsive loads could be useful to obtain a better definition of the overall structural load. However, the development of a detailed control procedure requires a huge effort and it has not yet been developed for the two configurations. For this reason, in the present analysis, the propulsive loads have been supposed as the worst-case scenarios of a command action very similar to the demonstrator one.

The structural analysis has been performed with the specific purpose of selecting the minimum length suitable to fulfil the described above requirements for each airship configuration. For this purpose, an iterative approach has been used to define the weight components. Some of the components, in fact, depend on the overall dimensions and weight of the airship, the latter being a function of the structural weight. For both the configurations, the iterative procedure has been triggered assuming an overall dimension for the airship; the weight has consequently been estimated in order to evaluate the weights and dimensions of the subsystems. Multiple iterations have been necessary to obtain a convergence value for each airship length. The minimum feasibility value, in fact, has been determined by gradually increasing the overall dimension and verifying whether the available buoyancy is enough to counteract the overall weight. The buoyancy that is needed to contrast the airship weight, in fact, increases proportionally with the cube of the length, whereas the structural weight increases roughly with its square. For this reason, the two configurations have both been parameterised with the airship length. In particular:

- the landing gear weight is estimated as 15 % of the total weight;
- for the power unit, the ratio weight on power is considered constant whereas the trend of the required power is assumed proportional to the airship inertia;
- the weight of the systems is estimated from empirical data as a function on the onboard power;
- the weight/power ratio of the propulsion electrical motors is considered constant;
- as far as the envelope weight is concerned, previous experience and data taken from the state-of-the-art surveys [21] suggest specific values of about 200 g/m^2 for the soap-shaped configuration and 300 g/m^2 for the double-hull;

In order to minimize the calculation costs, the structural analysis has been restricted to the most severe load conditions, which have been selected through the analysis of the operative conditions.

The structural comparison has been performed with the two configurations featuring the minimum required length.

A preliminary analysis, in fact, has revealed that the exoskeleton should have a minimum length of 32 m, whereas the double-hull length cannot be less than 36 m (Fig. 19). Moreover,

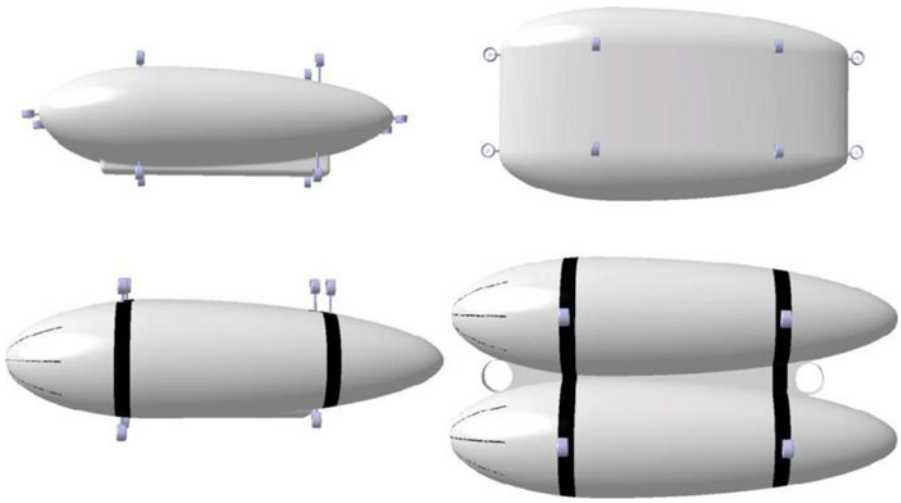

Fig. 19 Dimensional comparison between the two Nautilus ETF configurations

the closed structure, which is characteristic of the soap-shape exoskeleton configuration, has shown to be more effective in contrasting the external loads, which means that under the same maximum stress, the deformation peaks are reduced. However, the initial light solution of the T-section spars and ribs has demonstrated to be beneficial in terms of weight, but not in terms of local stresses and deformations.

The following load conditions have been used to compare the different solutions:

- Hovering—in this case the equilibrium of the vertical forces has been imposed: only a small amount of vertical throttle is used to compensate for the static weight. This case tests the resistance of the structure to the payload as well as the tendency of the structure to open under the static weight.
- Parking—This case simulates the parking condition (for two different configurations of the landing gears): the landing gears are extracted and the ground reactions are simulated. No external forces are applied.
- Vertical Engines—In this case, the vertical engine effects are simulated under their full throttle condition during an ascent, descent as well as during a pitch and a roll manoeuvre;
- Longitudinal Engines—In this case, the horizontal engines are simulated under their full throttle condition. Four different extreme load situations are investigated, in which the engines do not perform a specific manoeuvre, but stress the structure by pulling, bending (along two different axes) and twisting abnormally the airship;
- Crash—this condition investigates a heavy landing where the contact with the ground is only applied on one landing gear.

The structural analysis has been performed using two software packages: MSC.Patran [22] for the

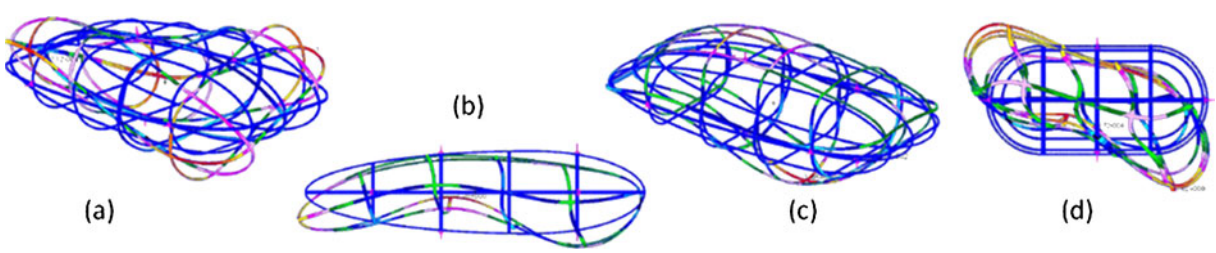

Fig. 20 First 4 structural modes: **a** torsional mode at 0,893 Hz; **b** flexural mode at 0,980 Hz; **c** second flexural mode at 1,206 Hz; **d** roll mode at 1,378 Hz

surface pre-processing and MSC.Nastran [23] for the structural calculations. The main problem of this kind of analysis is that the software requires the model to be somehow constrained, in order not to produce singular (non invertible) stiffness matrices. However, this problem could easily be avoided by adopting the *inertia relief* method. Inertia relief is an advanced option in Nastran, that allows an unconstrained structure to be simulated of under linear static conditions. This approach avoids the problem of unrealistic stress concentrations which would arise with conventional constraints. Typical applications of this method are the simulation of aircraft or satellites. According to the inertia relief hypothesis, the structure is unconstrained, and the structural inertia is considered to be able to resists the loads so that the entire structure is in a state of equilibrium. In an inertia relief simulation, the analyst selects a point in the structure which is used as a "support". The solver, then, applies a distribution of uniform accelerations which brings the system to a force and moment equilibrium. When the "inertia relief" option is invoked in a static analysis, MSC.Nastran calculates the resultant force in all directions, together with the field of acceleration that must be applied to the entire structure to reach the equilibrium.

- Modal Analysis

The dynamic structure behaviour, the impact of which has been investigated since the preliminary stage is an important factor. The first step is the determination of the structural natural modes and frequencies, to monitor and prevent dangerous interactions between low frequency structural vibrations and unsteady aerodynamic phenomena. As can be seen in the following sections, actually, the aerodynamic analysis has shown that a critical situation could arise for the hovering with lateral wind, when an aerodynamic vortex phenomenon is detached at a relatively low frequency (0.3 Hz). The modal analysis has focused on the first 20 natural modes, which span from 0,89 to 2,84 Hz, and are thus far from the aerodynamical vortex frequency of 0,3 Hz. Figure 20 shows the first 4 structural modes (besides the six free rotations and translations of the rigid body) which are then differently coupled in the high frequency modes.

The rotational speed of motors and propellers could affect the structural analysis and could potentially modify the structural modes or give rise to resonance problems. However, these effects have been neglected in the modal analysis.

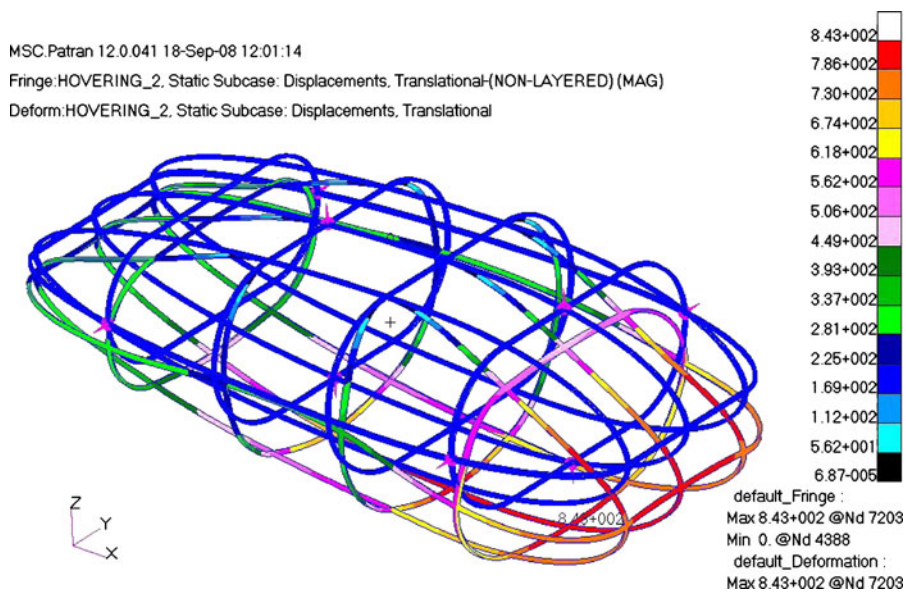

Fig. 21 Soap shape solution—hovering load case (the displacement values range from 0 to 843 mm)

- Displacements

A great number of linear static load cases have been analyzed during the structural analysis. The results have shown that, for the soap-shape configuration, deformations can cause displacements of almost one meter (Fig. 21), which can be accounted for as deformations of more than 3 % on the overall length of 32 m, and probably exceeds the theoretical limits of the linearity hypothesis.

In order to verify the validity of the linear assumptions, the results have been validated with the nonlinear analysis, which, however, has limited applicability, since it is not compatible with the inertia relief option. For this reason, a comparison was only possible for the parking test-case and for the vertical climb. Moreover, this approach, has been considered a higher-order analysis as it implies significantly higher computational costs than the linear approach. It was therefore decided to preliminarily evaluate the scale of displacements in every single case and then refine the analysis with the non-linear equations only in specific situations. The validation results for the exoskeleton configuration are summarized in Table 1.

Values show significant accordance, from which it can be deduced that the resultant deformations in the parking condition still comply with the condition of linearity, and that, as a consequence, the linear analysis can be considered validated. However, it must be noticed that these load conditions have been analysed imposing a solution based on the nonlinear displacements equations, in which the material characteristic parameters are considered linear, which is clearly an hypothesis excessively conservative. In order to reduce displacements on the soap-shape configuration on the most critical load conditions, it was decided to introduce a net of guy ropes that would allow the ventral loads to be distributed over the dorsal structural components. This expedient allows structure stiffness to be increased with a negligible increment in the overall weight.

As for the double-hull model, restraining straps were simulated to join the top and bottom ends of the supporting arms, in order to observe whether the displacements would still be as substantial. The results have shown that displacements relative to the two S-shaped arms are notably decreased. However, for the double-hull model the simulation was not entirely realistic, since the hulls themselves were not included, thus it was not possible to investigate how the restraining straps interacted with the membrane and the resultant stresses on both bodies.

Table 2 shows the results for the two models under different load conditions.

As can be noticed, the soap-shape configuration exhibits displacements that are within the acceptable limits of 500 mm for the majority of load cases. The guy ropes have greatly reduced the displacement levels, which are now very limited, compared to the overall exoskeleton size. The same conclusions apply to the double-hull configuration, for which the loads transmitted from the hulls to the saddles do not cause stress

Table 2 Displacement comparison between the exoskeleton and double-hull configurations

Load cases	Exoskeleton	Double-hull
	Displacements[m]	Displacements[m]
Hovering	0,132	0,336
Mot. Long. 1	0,147	0,354
Mot. Long. 2	0,149	0,340
Mot. Long. 3	0,147	0,971
Mot. Long. 4	0,144	0,752
Mot. Vert. 1	0,182	0,336
Mot. Vert. 2	0,115	0,344
Mot. Vert. 3	0,147	0,384
Mot. Vert. 4	0,144	//
Parking 1	0,533	//
Parking 2	0,773	0,307

Table 1 Comparison between the linear and nonlinear analysis for the exoskeleton configuration

Load case	Linear		Non linear	
	Displacement [m]	Stress [MPa]	Displacement [m]	Stress [MPa]
Mot. Vert. 1	1,15	1,120	1,3	1,260
Parking 1	0,533	435	0,491	434
Parking 2	0,733	810	0,855	877

and strain levels to an extent that could compromise the structural integrity. In order to verify the acceptability level of the displacements from a functional point of view, these values have been introduced into the dynamic ETF Flight Simulator to verify whether the airship is still able to maintain complete controllability even when the propellers position has changed due to structure deformation.

- Stress Analysis

The performed analysis has not highlighted any abnormal load concentration for the double-hull configuration. Conversely, the soap-shape structure features anomalous loading concentrations in the joint areas. This could be in part due to the lack of details in the connection modelling, which, at this stage, is usually kept very simple. The connections will be dealt with in more detail in a more advanced design phase whereas, at this point, the concentrated reactions are simply tolerated as a normal consequence of poor modelling.

In order to avoid misleading evaluations, the comparison has been performed with stresses generated in areas located at a proper distance from the joint and load concentrations. Generally speaking, the double-hull design performs particularly well, due to its optimum stress distribution, which does not exceed 300 MPa at any point of the structure. Conversely, the exoskeleton solution yields to critical stresses along the vertical axis, in particular in the parking configuration when the weight of the structure is counteracted by the ground constraints. However, the analysis of this comparison does not take into account the alleviating effect of the buoyancy, which can reduce the load by 5 % in operational conditions. It should be considered, however, that during construction, alleviating forces from the propellers and buoyancy are not present, so the structure could indeed experience the magnitudes of the calculated stress that results from its own weight.

Table 3 shows the results of the inertia relief analysis for various load situations.

The stress magnitude for the exoskeleton could easily be reduced by increasing the rib thickness. This expedient has the obvious drawback of increasing the weight of the structure, and could cause further problems for the production, transportation and construction. An optimisation study could alternatively be performed to identify the best section shape, featuring low weight per unit length and high inertia at the same time. In this context, for example, the closed square section would be much more effective that the T-shape, and would only introduce a modest weight increment.

Table 3 Stress comparison between the exoskeleton and double-hull configurations

Load cases	Exoskeleton	Double-hull
	Stress [MPa]	Stress [MPa]
Hovering	353	144
Mot. Long. 1	367	193
Mot. Long. 2	346	269
Mot. Long. 3	354	280
Mot. Long. 4	364	264
Mot. Vert. 1	375	133
Mot. Vert. 2	354	155
Mot. Vert. 3	369	163
Mot. Vert. 4	1,120	//
Parking 1	435	//
Parking 2	810	137

8 Conclusions

In this paper two airship configurations for the Elettra Twin Flyer prototype have been analyzed and compared: the first, a double-hull solution, is characterised by a main structure, connected to the two gas envelopes by means of a set of elongated S-shape clamps. The second solution, the soap-shaped or exoskeleton design, consists of a rigid structure featuring a single hull formed by the union of two parallel hulls, supported internally by a system of structural ribs.

Numerical analyses have revealed that there is a distinct advantage, from an aerodynamic point of view, for the soap-shape design, in particular in the "cross-wind" situation (hovering with air flow perpendicular to the longitudinal symmetrical plane, as shown in Fig. 12). Table 4 shows how the comparison has been structured within the cost function, as described in one of the previous sections: six factors have been recognized as being critical and weighted in the cost function, through a weight index ranging from 0.2 to 1, depending

Table 4 Cost function evaluation

Factor	Parameter	Weight index	Soap-shape	Double-hull	Soap-shape	Double-hull
Overall dimension	Minimum overall length [m]	medium-high	32	36	1	1.125
Weight	Structural mass, total mass [kg] (50 %/50 %)	medium-low	998/2,680	1,200/3,053	1	1.171
Wind sensitivity	C_x at $\beta = 90°$	high	0.28	0.55	1	1.964
Handling	Structure length [m]	medium	32	22	1.454	1
Acquisition and operating costs	moulds, pieces, joints (50 %/30 %/20 %)	medium-high	14/120/38	6/23/54	2.932	1.084
Reliability, service life and maintenance	–	medium-high	–	–	–	–
Cost function					1.084	1.339

on the impact level (from low to high) associated to each aspect. A parameter has been selected to numerically quantify each factor: for example, the acquisition and operating costs have been translated into number of moulds, pieces and joints which must be produced for each configuration, considering an autoclave with a limited volume of $5 \times 3 \times 0.5$ m. These three numbers have a different impact on the acquisition and operating costs, as it would obviously be more cost-effective to have a low number of moulds, in primis. For this reason, 50 % of the related parameter is constituted by the number of moulds, whereas the number of pieces accounts for just 30 % of the same factor.

All the parameters selected to represents the different factors must be minimized and for this reason it has been decided to scale them on the basis of the lower value obtained for the two configurations: in this way, the optimal value is always the unit, regardless of the physical meaning, whether kilograms or meters. The resulting non-dimensional parameters have been weighted and added together linearly or quadratically (as for the wind sensitivity parameter) in the cost function: the closer the cost function to the unit value, the better the configuration. In short, the cost function reveals that the structural and financial advantages of the double-hull configurations are roughly balanced by the aerodynamic benefits of the soap-shape design.

Important parameters in this preliminary analysis, such as the economic impact of ground structures for the airship assembly and operation, or of the helium handling, refilling/washing, have been omitted from the cost function. The evaluation of these parameters has been considered too vague and arbitrary at this stage, but should surely be performed, through a market survey, during the engineering process. The most important parameters have been thoroughly evaluated in this preliminary analysis and have led to

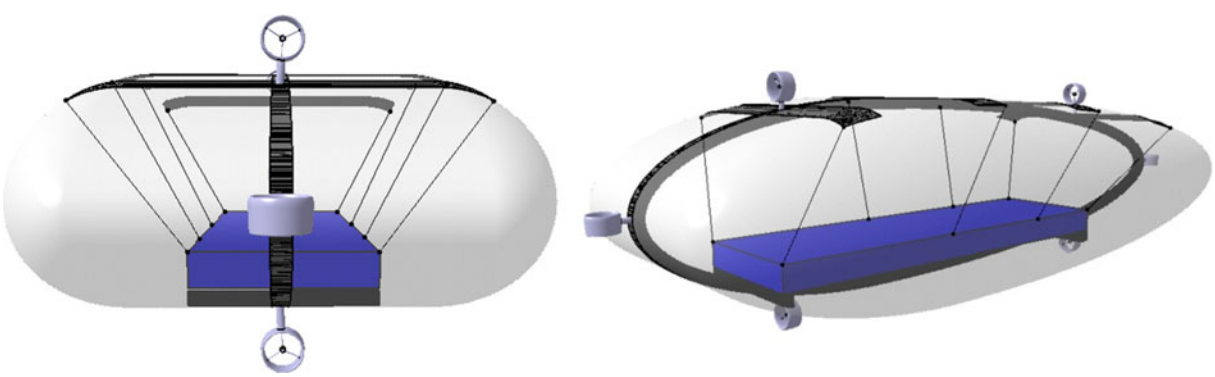

Fig. 22 The new structural solution

interesting conclusions, according to which a third design (Fig. 22) can be considered worth evaluating. This design actually represents an improvement of both the configurations, as it unites the aerodynamic advantages of the soap-shape design to the construction benefits of the double-hull. Figure 21 shows the internal cables and supports used to pull the internal bladder in order to preserve the soap shape. A robust longitudinal keel has been introduced, as the only rigid structural element on which all the loads are concentrated, including propulsive, aerodynamic and buoyancy forces. The command and control systems remain unchanged.

Acknowledgements The joint academic-private firm research activity presented in the paper has been developed within the ETF06 project funded by the Regione Piemonte, Italy.

Appendix 1: List of Notations

$C_{x,y,z}$	Aerodynamic force coefficients
$C_{Mx,My,Mz}$	Aerodynamic moment coefficients in body axis
Cp_{tot}	Total pressure coefficient
D	Hull diameter
F_X, F_Y, F_Z	Total forces
I_x, I_y, I_z	Main inertia moments
I_{xy}, I_{xz}, I_{yz}	Products of inertia
J_x, J_y, J_z	Apparent main inertia moments
J_{xy}, J_{xz}, J_{yz}	Apparent products of inertia
L, M, N	Rolling, pitching and yawing moments
$\mathring{L}_{\dot{p}}, \mathring{M}_{\dot{q}}, \mathring{N}_{\dot{r}}$	Gas main inertia moments
$\mathring{L}_{\dot{q}}, \mathring{N}_{\dot{p}}, \mathring{M}_{\dot{r}}$	Gas products of inertia
$\mathring{M}_{\dot{p}}, \mathring{L}_{\dot{r}}, \mathring{N}_{\dot{q}}$	Gas products of inertia
R	Propeller radius
T	Thrust
T_K	Absolute temperature
U	Free-stream airspeed
V	Volume of the hulls
X, Y, Z	CG reference frame
$\mathring{X}_{\dot{u}}, \mathring{Y}_{\dot{v}}, \mathring{Z}_{\dot{w}}$	Gas masses
b_x, b_z	Coordinates of the center of buoyancy
g	Gravity acceleration
l	Reference length of the wet surface
m	Mass
m_x, m_y, m_z	Apparent masses
n	propeller rotational speed in rounds per minutes (RPM)
p, q, r	Components of the angular rate
p_a	Atmospheric pressure
$\dot{p}, \dot{q}, \dot{r}$	Components of the angular acceleration
u, v, w	Components of the translation velocity
$\dot{u}, \dot{v}, \dot{w}$	Components of the translation acceleration
Λ	Specific weight
α	Angle of attack
β	Sideslip angle
γ	Climb angle
ε	Specific weight ratio
ϕ, ϑ, ψ	Euler angles
η	Functioning point
ρ	Air density
ω	Propeller angular rate

References

1. Inventors: Gili, P.A., Battipede, M., Icardi, U., Ruotolo, R., Vercesi, P., Owner: Nautilus S.p.A., Politecnico di Torino: Dual hull airship controlled by thrust vectoring, N. PCT/EP03/08950 (2003)
2. Elfes, A., Bueno, S.S., Bergerman, M., Ramos, J.G., Jr.: A semi-autonomous robotic airship for environmental monitoring missions. In: Proceedings of the 1998 IEEE International Conference on Robotics & Automation. Leuven, Belgium, pp. 3449–3455 (1998)
3. Zaugg, D.A., Arnold, D.V., Jensen, M.A.: Ocean surface and landside probing with a scanning radar altimeter. In: Proceedings of the 2000 International Geoscience and Remote Sensing Symposium, vol. 1, pp. 120–120 (2000)
4. Hain, J.H.W.: Lighter-than-air platforms (Blims and Aerostats) for oceanographic and atmospheric research and monitoring. In: Proceedings of the Oceans 2000 MTS IEEE Conference and Exhibition, vol. 3, pp. 1933–1936 (2000)
5. Battipede, M., Lando, M., Gili, P.A., Vercesi, P.: Peculiar performance of a new lighter-than-air platform for monitoring. In: Proceedings of the AIAA Aviation Technology, Integration and Operation Forum. AIAA, Reston, VA (2004)
6. Battipede, M., Gili, P.A., Lando, M.: Prototype assembling of the nautilus remotely-piloted lighter-than-air platform. In: Proceedings of the AIAA Aviation

Technology, Integration and Operation Forum. AIAA, Reston, VA (2005)
7. Battipede, M., Gili, P.A., Lando, M.: Control allocation system for an innovative remotely-piloted airship. In: Proceeding of the Atmospheric Flight Mechanics Conference. AIAA, Reston, VA (2004)
8. Battipede, M., Gili, P.A., Lando, M., Gunetti, P.: Flight control system rapid prototyping for the remotely-piloted Elettra-Twin-Flyer airship. In: Proceeding of the AIAA Modeling and Simulation Technologies Conference and Exhibit. AIAA, Reston, VA (2006)
9. Gili, P., Battipede, M., Vazzola, M., Cassino, P.: Ground testing of the ETF unmanned airship technology demonstrator. In: Proceeding of the AeroTech—Unmanned Aerial Systems Conference, Toulouse, Fr, 18–21 October 2011. Warrendale, PA 15096–0001—US: SAE International (2011) doi:10.4271/2011-01-2589
10. Erlander, Sven, B.: Cost-minimizing choice behavior in transportation planning. 1st Edn. Springer 2010. XII, ISBN: 978-3-642-11910-1 (2010)
11. Cappadona, A., Lecca, R., Vazzola, M., Gili, P.A., Farina, P., Surace, C.: Innovative unmanned airship structural analysis: double-hull and exoskeletal configurations. In: Proceedings of the 7th International Conference on Modern Practice in Stress and Vibration Analisys. New Hall, Cambridge, UK, 8–10 September (2009)
12. Battipede, M., Gili, P., Vazzola, M.: Structure design for the Elettra Twin Flyers prototype. In: Proceedings of the 24th Bristol International Unmanned Air Vehicle System Conference. Bristol, UK, 30th March–1st April (2009)
13. Narayana C.L., Srilatha, K.R.: Analysis of aerostat configurations by panel methods, NAL PD CF 0010, Technical Report, National Aerospace Laboratories, Bangalore, India, July (2000)
14. Lutz, T., Schweyher, H., Wagner S.: Shape optimization of axi-symmetric bodies in incompressible flow. J. Aircr. **20**, 520–526 (1985)
15. Visone M.: ETF06 airship aerodynamic investigations. Regione Piemonte ETF06 Project proceedings (2009)
16. STAR-CCM+User Guide
17. Patankar, S.V., Spalding, D.B.: A calculation procedure for heat, mass and momentum transfer in three-dimensional parabolic flows. Int. J. Heat Mass Transfer. **15**(10), 1787–1806 (1972)
18. Battipede, M., Gili, P.A., Lando, M., Massotti, L.: Flight simulator for the control law design of an innovative remotely- piloted airship. Proceedings of the AIAA Modeling Simulation and Technologies Conference, AIAA, Reston, VA (2004)
19. Rizzo, F.: A study of static stability of airships, NACA-TN-204 (1924)
20. Battipede, M., Gili, P., Lando, M.: Mathematical modeling of an innovative unmanned airship for its control law design. In: Ceragioli, F., Dontchev, A., Marti, K., Pandolfi, L. (eds.) IFIP International Federation for Information Processing, System, Control Modeling and Optimization, vol. 202, pp. 31–42. Boston Springer (2006)
21. Airship technology. In: Khoury, G.A., Gillett, J.D. (eds.) Cambridge Aerospace Series, February 28, 1999, ISBN-10: 0521430747, ISBN-13: 978–0521430746 (1999)
22. MSC Patran: FEM Pre and Post-Processing Software. MSC Software, USA (2005)
23. MSC Nastran: Finite Element Method (FEM) Software. MSC Software, USA (2005)